30th Annual International IEEE EMBS Conference
Vancouver, British Columbia, Canada, August 20-24, 2008

Multi-Feature Contour Evolution for Automatic Live Cell Segmentation in Time Lapse Imagery

Ilker Ersoy and Kannappan Palaniappan

Abstract— **Cell boundary segmentation in live cell image sequences is the first step towards quantitative analysis of cell motion and behavior. The time lapse microscopy imaging produces large volumes of image sequence collections which requires fast and robust automatic segmentation of cell boundaries to utilize further automated tools such as cell tracking to quantify and classify cell behavior. This paper presents a methodology that is based on utilizing the temporal context of the cell image sequences to accurately delineate the boundaries of non-homogeneous cells. A novel flux tensor-based detection of moving cells provides initial localization that is further refined by a multi-feature level set-based method using an efficient additive operator splitting scheme. The segmentation result is processed by a watershed-based algorithm to avoid merging boundaries of neighboring cells. By utilizing robust features, the level-set algorithm produces accurate segmentation for non-homogeneous cells with concave shapes and varying intensities.**

I. Introduction

Time lapse video microscopy in high troughput screening environments produces terabyte sized biological image sequence collections for unraveling cellular mechanisms, screening for biomarkers, drug discovery, image-based bioinformatics, etc. [1], [2]. Quantitative movement analysis of tissues, cells, organelles or molecules is one of the fundamental signals of biological importance. Live cell imaging in particular is undergoing a paradigm shift from the study of isolated, static, equilibrium macromolecular properties to disease contextual, dynamic, non-equilibrium cellular states and pathways [2], [3]. Algorithm development for the mining of video microscopy data presents new challenges which require scalable techniques for feature extraction, classification, clustering, and indexing [4]. Challenging aspects in the development of robust scalable algorithms for automated analysis of video microscopy imagery include large structural and feature variation in biological objects from molecular to organ level, large variation in morphology often lacking crisp boundaries, highly deformable movement, split-merge behavior, touching, overlapping or aggregated objects, etc. Another challenging aspect includes accommodating variation in image acquisition including platform positioning jitter, focus, illumination, environmental (i.e. non-homogeneous plate moisture) variations, This paper describes the flux tensor level set framework that effectively handles biological video segmentation in terms of accurate detection and segmentation of non-homogeneous cells in presence of complex biological processes, background noise and clutter. Section 2 describes the flux tensor-based moving object detection, section 3 describes multi-feature level set segmentation algorithm, section 4 describes the cluster segmentation algorithm to handle the merged boundaries of neighboring cells. Experimental results are given in section 5 and section 6 concludes the paper.

Research partially supported by the US NIH NIBIB award R33-EB00573.
Authors are with the Department of Computer Science, University of Missouri-Columbia, Columbia, MO 65211, USA.

II. Detecting Moving Cells Using the Flux Tensor

In this section we describe the flux tensor for accurate detection of moving cells in time lapse images. Under the constant illumination model, the optic flow equation of a spatiotemporal image volume $\mathrm{I}(\mathbf{x})$ centered at location $\mathbf{x} = (x, y, t)$ is given by,

$$\frac{d\mathrm{I}(\mathbf{x})}{dt} = \nabla \mathrm{I}(\mathbf{x}) \cdot \mathbf{v}(\mathbf{x}) = 0 \tag{1}$$

where $\cdot$ is the inner product operator between vectors and $\mathbf{v}(\mathbf{x}) = [v_x, v_y, v_t] = [\frac{\partial x}{\partial t}, \frac{\partial y}{\partial t}, v_t]$ is the optic flow vector at $\mathbf{x}$. In order to estimate $\mathbf{v}(\mathbf{x})$, Eq. 1 is minimized over a local 3D image volume centered at $\mathbf{x}$, and filtered using the convolution kernel $W(\mathbf{x}, \mathbf{y}, \sigma_I)$, subject to the condition that the orientation vector is of unit length $||\mathbf{v}(\mathbf{x})|| = 1$. This leads to the standard minimum eigenvalue problem, $\mathbf{J}(\mathbf{x}, W)\hat{\mathbf{v}}(\mathbf{x}) = \lambda\hat{\mathbf{v}}(\mathbf{x})$. For the best estimate of $\mathbf{v}(\mathbf{x})$, it is shown that $\mathbf{J}(\mathbf{x}, W) = \int\{\nabla \mathrm{I}(\mathbf{y}, \sigma_D)\nabla \mathrm{I}^T(\mathbf{y}, \sigma_D)\}W(\mathbf{x} - \mathbf{y}, \sigma_I)\, d\mathbf{y}$ which is the integral of an outer product matrix where σ_D is a scale parameter of gradient computation. This is the classical 3D grayscale structure tensor for the spatiotemporal window centered at $\mathbf{x}$. The shortcoming of the structure tensor is that, although the elements of $\mathbf{J}$ include information relating to gradient changes, the temporal variation of these gradients is not fully incorporated. Recently we have developed an extension of the grayscale structure tensor for motion detection known as the flux tensor [6] and its application to segmenting motile cells [7]. Under the brightness constancy and locally constant velocity model, the partial derivative of Eq. 1 with respect to t,

$$\frac{\partial}{\partial t}\frac{d\mathrm{I}(\mathbf{x})}{dt} = \nabla_t \mathrm{I}(\mathbf{x}) \cdot \mathbf{v}(\mathbf{x}) + \nabla \mathrm{I}(\mathbf{x}) \cdot \mathbf{a}(\mathbf{x}) \tag{2}$$

where the spatiotemporal derivative operator is defined as, $\nabla_t \equiv \frac{\partial}{\partial t}\nabla$, $\mathbf{v}(\mathbf{x})$ is the velocity field and $\mathbf{a}(\mathbf{x}) = [a_x, a_y, 0]$ is the acceleration of the pixel at $\mathbf{x}$. We use a locally constant motion model for $\mathbf{v}(\mathbf{x})$, as in the traditional structure tensor, and the error functional simplifies to $e^{\mathrm{F}}_{ls}(\mathbf{x}) = \int\{\nabla_t \mathrm{I}(\mathbf{y}, \sigma_D) \cdot \mathbf{v}(\mathbf{x})\}^2 W(\mathbf{x}, \mathbf{y}, \sigma_I)\, \mathbf{y} + \lambda\{1 - \mathbf{v}(\mathbf{x}) \cdot \mathbf{v}(\mathbf{x})\}$.

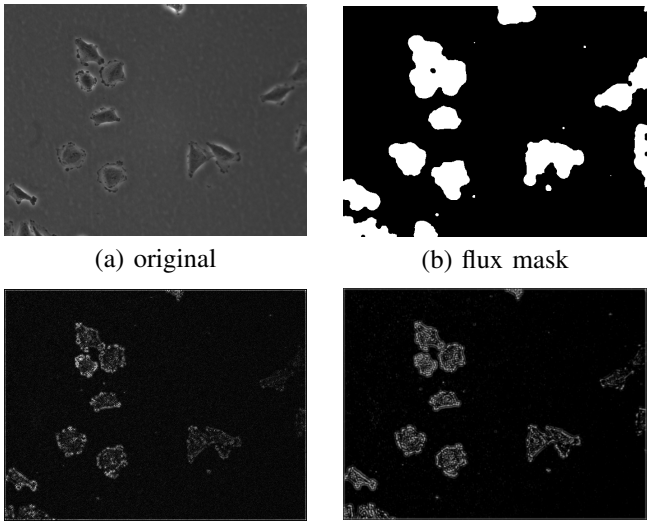

(a) original (b) flux mask

(c) variance (d) Hamming texture

Fig. 1: Frame 165 from human melanoma cells in a control experiment (data from [3]).

Similar to the 3D grayscale structure tensor, $\mathbf{J}$, we denote the tensor quantity, $\mathbf{J_F}$, as the *flux tensor* which is the filtered temporal variation of the image gradient fields using spatially invariant convolution: $\mathbf{J}_{\mathrm{F}}(\mathbf{x}, W) = \int \{\nabla_t \mathrm{I}(\mathbf{y}, \sigma_D)\, \nabla_t^T \mathrm{I}(\mathbf{y}, \sigma_D)\}\, W(\mathbf{x}-\mathbf{y}, \sigma_I)\; d\mathbf{y}$. The flux tensor $\mathbf{J_F}$ can be written in expanded matrix form (Eq. 3) and the trace of $\mathbf{J}_{\mathrm{F}}$ gives a motion energy map that is sufficient to discriminate between moving and stationary portions of the scene without expensive eigen-decomposition analysis.

$$\mathbf{J_F} = \begin{bmatrix} \int\limits_{\Omega} \left\{\frac{\partial^2 \mathbf{I}}{\partial x \partial t}\right\}^2 d\mathbf{y} & \int\limits_{\Omega} \frac{\partial^2 \mathbf{I}}{\partial x \partial t}\frac{\partial^2 \mathbf{I}}{\partial y \partial t} d\mathbf{y} & \int\limits_{\Omega} \frac{\partial^2 \mathbf{I}}{\partial x \partial t}\frac{\partial^2 \mathbf{I}}{\partial t^2} d\mathbf{y} \\ \int\limits_{\Omega} \frac{\partial^2 \mathbf{I}}{\partial y \partial t}\frac{\partial^2 \mathbf{I}}{\partial x \partial t} d\mathbf{y} & \int\limits_{\Omega} \left\{\frac{\partial^2 \mathbf{I}}{\partial y \partial t}\right\}^2 d\mathbf{y} & \int\limits_{\Omega} \frac{\partial^2 \mathbf{I}}{\partial y \partial t}\frac{\partial^2 \mathbf{I}}{\partial t^2} d\mathbf{y} \\ \int\limits_{\Omega} \frac{\partial^2 \mathbf{I}}{\partial t^2}\frac{\partial^2 \mathbf{I}}{\partial x \partial t} d\mathbf{y} & \int\limits_{\Omega} \frac{\partial^2 \mathbf{I}}{\partial t^2}\frac{\partial^2 \mathbf{I}}{\partial y \partial t} d\mathbf{y} & \int\limits_{\Omega} \left\{\frac{\partial^2 \mathbf{I}}{\partial t^2}\right\}^2 d\mathbf{y} \end{bmatrix} \quad (3)$$

The filters proposed in [5] are used for accurate computation of the gradient fields in $\mathbf{J}_{\mathrm{F}}(\mathbf{x})$. Flux tensors $\mathbf{J}_{\mathrm{F}}(\mathbf{x})$ are estimated for each pixel over an isotropic local 3D neighborhood centered at location $\mathbf{x}$ in the image $\mathrm{I}(\mathbf{x})$ weighted by a Gaussian function for the convolution integral. The 3D convolutions for both the derivative and smoothing filters are efficiently implemented as separable 1D convolutions with two FIFO buffers that store intermediate results for reuse in temporal direction to reduce computational requirements. The detection performance of flux tensor has been demonstrated in surveillance sequences as well as biological sequences [6], [7]. Flux tensor response encapsulates the spatio-temporal area of detected motion, hence detection in a single frame is larger than the detected cells themselves and is elongated along the direction of motion. We use the flux tensor response to accurately initialize the curve evolution in a region that is close to the desired segmentation and to guarantee that the evolution starts from outside of the cells.

III. Multi-feature Geodesic Active Contour Level Set Segmentation

Level set-based segmentation methods provide an implicit representation of the evolving contour and can gracefully handle the toplogical changes during the evolution. One widely used level set-based algorithm to segment 2D images into two classes was proposed by Chan and Vese [8] and is well suited for segmenting nearly homogeneous biological objects which often do not have distinct edges as discussed in [9]. The original Chan and Vese formulation enforces a homogeneity constraint on the segmented regions in terms of the average gray value. This effectively evolves the curve to find the interface which separates darker regions from lighter regions without requiring strong edges. This assumption is not satisfied in microscopic imagery where in some phase contrast microscopy images of cells, the average cell gray value is not significantly different from the background (as seen in Figure 1) and phase halos (bright regions adjacent to cell boundaries) are of the same intensity as rounded-up cells beginning mitosis. The nuclei of cells also do *not* exhibit significantly different features that would enable nucleus segmentation and subsequently curve evolution schemes initialized by locations of nuclei [10]. Features that can differentiate the cells from the surroundings are required for robust segmentation such as distributions of image variance, texture and shape. Edges are also important image features that can be integrated into an active contour approach trough the use of an edge-stopping function [11]. By combining a multi-feature formulation based on a Bayesian inference approach [12] with terms for geodesic length and area, we obtain

$$\begin{aligned} E(p_{1j}, p_{2j}, \phi) = -\sum_{j=1}^{N} \Bigg(& \lambda_{1j} \int_{\Omega} \log p_{1j}\big(\mathrm{I}_j(\mathbf{x})\big) H\big(\phi(\mathbf{x})\big)\, d\mathbf{x} \\ & + \lambda_{2j} \int_{\Omega} \log p_{2j}\big(\mathrm{I}_j(\mathbf{x})\big) \Big(1 - H\big(\phi(\mathbf{x})\big)\Big)\, d\mathbf{x} \Bigg) \\ & + \mu \int_{\Omega} g |\nabla H\big(\phi(\mathbf{x})\big)|\, d\mathbf{x} + \nu \int_{\Omega} g H\big(\phi(\mathbf{x})\big)\, d\mathbf{x} \end{aligned} \quad (4)$$

where p_{ij} corresponds to the conditional probability density function of observing feature value $\mathrm{I}_j(\mathbf{x})$ within region Ω_i (i.e. for two classes interior and exterior), $\phi(\mathbf{x})$ is the embedding Lipschitz functional, $H(\phi)$ is a regularized Heaviside function used to define the interior and exterior regions of level set contours, the μ term is the geodesic length of all contours and the ν term is the geodesic area where g is a 2D edge stopping function. Minimizing this functional with respect to ϕ leads to the associated Euler-Lagrange equations and provides a gradient descent update equation for the contour evolution:

$$\begin{aligned} \frac{\partial \phi}{\partial t} = & \; \delta(\phi) \sum_{j=1}^{N} \Big(\lambda_{1j} \log\, p_{1j}\big(\mathrm{I}_j(\mathbf{x})\big) - \lambda_{2j} \log\, p_{2j}\big(\mathrm{I}_j(\mathbf{x})\big) \Big) \\ & + \delta(\phi) \Big(\mu \,\mathrm{div}\, g \frac{\nabla \phi}{|\nabla \phi|} + \nu g \Big) \end{aligned} \quad (5)$$

The speed of convergence and stability of the contour evolution depends on factors such as the initialization of ϕ, the

size of the evolution time step Δt and the numerical update schemes. When the gradient descent equation is solved using an explicit numerical scheme, the time steps need to be relatively small for stable convergence (e.g. $\Delta t = 0.1$) in order to satisfy the Courant-Friedrichs-Levy condition and hundreds of iterations are needed to converge to an accurate solution. By using the flux tensor response, the geodesic terms and a semi-implicit numerical implementation, we obtain a fast scheme that can converge to accurate boundaries in 50–100 iterations. The geodesic area term provides an additional constant force that shrinks the contour until it reaches to an edge. Usage of this term requires the initialization of ϕ in such a way that the initial curve is outside the cells in the image. The thresholded trace of the flux tensor, as described before, is used as the initial mask for the level set evolution. This reduces the number of iterations significantly and guarantees that the initial curve starts from outside the cells, enabling the use of the constant force which further speeds up the convergence. The robust multi-feature formulation balances the energy where edge-stopping fails due to weak gradients. In [13] a semi-implicit scheme named *additive operator splitting* (AOS) was derived for non-linear diffusion filtering that is numerically stable for large time steps (e.g. $\Delta t = 30$). We derive the AOS update equations for Eq. 5 since it is of the same form as $\frac{\partial \phi}{\partial t} = a(\phi) + \mathrm{div}(b(\phi)\nabla\phi)$ leading to an efficient implementation. We refer the reader to [14] for a description of a similar AOS derivation for Chan and Vese functional. The robust features we employ for this type of data are the image variance and the Hamming texture. The Hamming texture we propose is similar to the rank transform in [15], it provides a robust measure of intensity variation that is less sensitive to illumination change. The Hamming texture measure for a pixel $I(x, y)$ at the center of a $n \times n$ neighborhood is defined as the cardinality of the set

$$\Big\{ I(i,j) \mid I(i,j) - I(x,y) > gap,\ \forall\, i \neq x,\ j \neq y \quad \text{where } i \in [x - \frac{n}{2}, x + \frac{n}{2}],\ j \in [y - \frac{n}{2}, y + \frac{n}{2}] \Big\} \qquad (6)$$

The neighborhood and gap are chosen as 5×5 and 0.06 respectively.

IV. Cell Cluster Segmentation

Evolving the level set-based active contours from the initial motion mask toward cell boundaries results in tighter cell contours, but neighboring or touching cells in certain frames may not be separated by the contour because of the lack of adequate spacing in between, or because of the early stopping due to weak inside-outside energy difference. In such cases the process leads to under-segmentation where clusters of cells are merged into a single object. We employ a cell cluster segmentation and validation algorithm to break clusters into individual cells by enforcing separation based on previous segmentation $\mathrm{M}(t\text{–}1)$. In general, two methods can be considered to break up clusters: 1) Static barriers obtained from generalized voronoi diagram of the combined mask $\mathrm{M}(t\text{–}1) \cap \mathrm{M}(t)$. 2) Marker-controlled watershed segmentation on distance transform on the current mask $-Dist(\mathrm{M}(t))$.

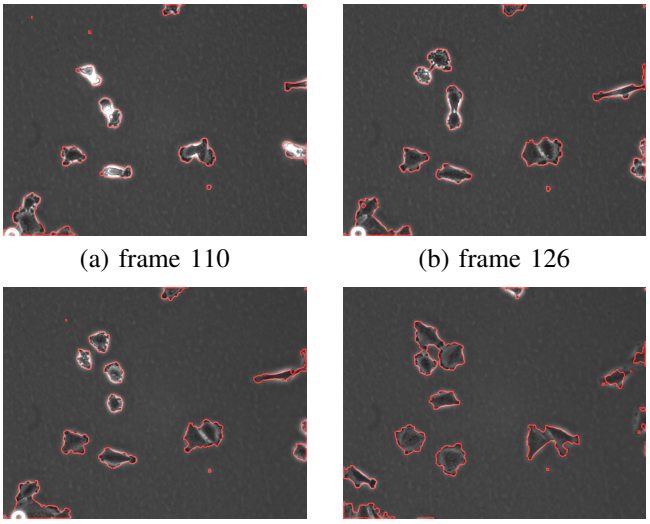

(a) frame 110 (b) frame 126

(c) frame 130 (d) frame 165

Fig. 2: Segmentation results: in different stages of division, cells exhibit different characteristics (circular and brighter in prophase/metaphase, flattened out, elongated and textured in anaphase/telophase/interphase).

These methods have their drawbacks: static barriers method can not handle large displacements of cells, watershed on distance transform tends to break-up clusters at their narrowest region so it fragments narrow elongated cells. We employ a more robust marker-controlled watershed segmentation based on fusion of image intensity and distance transform on the current mask $\alpha I(t)$–$(1\text{–}\alpha)Dist(\mathrm{M}(t))$. This method incorporates more relevant information, thus produces more accurate segmentation. It tends to break-up clusters on narrow regions with phase halos, which generally coincide with actual cell borders. The use of markers prevents over-segmentation and enables incorporation of segmentation results from the previous frame thus enforcing the correct number cells. False fragmentation is prevented by employing a two step partition validation algorithm: 1) before cluster segmentation, each disjoint region in $\mathrm{M}(t)$ is validated by checking parent regions in $\mathrm{M}(t\text{–}1)$. Cluster segmentation is activated only on regions of $\mathrm{M}(t)$ with multiple parents, 2) after cluster segmentation, the partitioning is validated using a heuristic based on maximum, minimum and relative sizes of the obtained partitions.

V. Results

The proposed method was applied to human melanoma cells. The local image variance and the Hamming texture measure are chosen as the robust features for this type of cells since the cells have visibly different variance and texture from the background whereas intensity does not constitute a discriminating feature. Figure 1 shows a sample frame from one field in the T25 plastic culture flask of a control experiment with a low density culture of human melanoma cell line WM793 to assess any toxicity to the high-throughput imaging system [3]. Pixel resolution is 0.67 micron $\times\, 0.59$

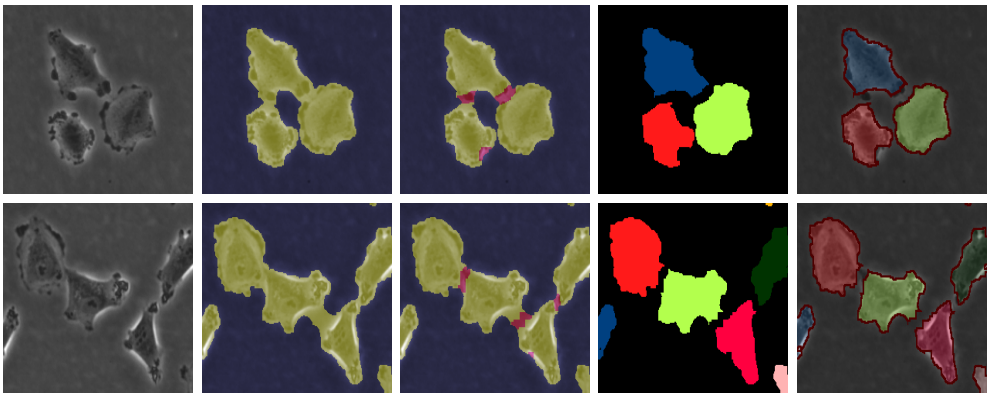

Fig. 3: Cluster segmentation results using marker-controlled watershed on intensity and distance fusion, details of frames 165 (top) and 261 (bottom). Left to right: original image, active contour segmentation result, cluster segmentation result (yellow: mask, red: watershed barrier), separated cells, final segmentation on original.

micron in X and Y using a $20\times$ objective lens. The flux tensor detects moving cells reliably and provides an initial mask. The images are normalized before segmentation in order to reduce the effect of phase halos by dividing each image by its smoothed version. Using the combination of local image variance and the texture measure leads to successful segmentation together with the geodesic terms. Some of the cells in these sequences do not exhibit sharp boundaries so geodesic active contours alone would not produce reliable cell segmentation. Using the flux tensor initialization and the semi-implicit AOS scheme with $\Delta t = 30$, the level set segmentation converges in 50–100 iterations. The parameters of the level set are following: $\lambda_{11} = \lambda_{21} = 0.05, \lambda_{12} = \lambda_{22} = 0.0005, \mu = 20, \nu = 4$. Figure 2 shows segmentation results, the complex contours of the three dividing cells are accurately extracted from the initial compact bright rounded-up circular stage through elongated dark flattened-out post-cytokinesis final stages. The divided cells touch each other and form a cluster in the subsequent frames which is handled by the proposed cluster segmentation algorithm to enforce the correct number of blobs based on previous frames as shown in Figure 3.

VI. Conclusions and Future Work

A new flux tensor-based motion detection and multi-feature level set segmentation algorithm was developed for the segmentation of motile biological objects suitable for high-througput live cell microscopy studies. The proposed algorithm can handle non-homogeneous biological objects undergoing complex split-merge deformations, which continues to be a challenging research area. The flux tensor, compared to the structure tensor, is able to differentiate between stationary and non-stationary moving image features without requiring eigen-decompositions. It detects moving objects and provides a good initialization close to the ideal contour that is also outside the object enabling the use of geodesic terms. Edge, variance and texture features provide a robust and fast segmentation. The AOS implementation further increases the computational efficiency. Neighboring cells that merge due to weak energy are effectively separated by a robust marker-controlled watershed algorithm. Future work includes improving the marker-controlled separation by feedback from cell tracking module and evaluating further texture and edge measures as candidate features in the segmentation process.

References

[1] A.Carpenter, T.Jones, M.Lamprecht, C.Clarke, I.Kang, O.Friman, D.Guertin, J.Chang, R.Lindquist, J.Moffat, P.Golland, and D.Sabatini, "CellProfiler: Image analysis software for identifying and quantifying cell phenotypes," *Gen. Bio.*, vol. 7, no. 10, 2006.

[2] U. S. Eggert and T. J. Mitchison, "Small molecule screening by imaging." *Curr. Opin. Chem. Biol.*, vol. 10, no. 3, pp. 232–237, 2006.

[3] P. Davis, E. Kosmacek, Y. Sun, F. Ianzini, and M. Mackey, "The large scale digital cell analysis system: An open system for non-perturbing live cell imaging," *J. Microscopy*, vol. 228, no. 3, pp. 296–308, 2007.

[4] X. Zhou and S. Wong, "High content cellular imaging for drug development," *IEEE Trans. Signal Process.*, vol. 23, no. 2, pp. 170–174, Mar. 2006.

[5] F.Bunyak, K.Palaniappan, S.Nath, and G.Seetharaman, "Flux tensor constrained geodesic active contours with sensor fusion for persistent object tracking," *J. Multimedia*, vol. 2, no. 4, pp. 20–33, 2007.

[6] K.Palaniappan, I.Ersoy, and S.Nath, "Moving object segmentation using the flux tensor for biological video microscopy," in *LNCS - Proc. PCM 2007*. Springer, 2007, vol. 4810, pp. 483–493.

[7] H.Farid and E.Simoncelli, "Differentiation of multidimensional signals," *IEEE Trans. Image Process.*, vol. 13, no. 4, pp. 496–508, 2004.

[8] T.Chan and L.Vese, "Active contours without edges," *IEEE Trans. Image Process.*, vol. 10, no. 2, pp. 266–277, Feb. 2001.

[9] F.Bunyak, K.Palaniappan, S.K.Nath, T.I.Baskin, and G.Dong, "Quantitative cell motility for *in vitro* wound healing using level set-based active contour tracking," in *Proc. 3^{rd} IEEE Int. Symp. Biomed. Imaging (ISBI)*. IEEE Comp. Soc., April 2006, pp. 1040–1043.

[10] P.Yan, X. Zhou, M. Shah, and S. Wong, "Automatic segmentation of high throughput RNAi fluorescent cellular images," *IEEE Trans. Inf. Tech. Biom.*, vol. 12, no. 1, pp. 109–117, 2008.

[11] V.Caselles, R.Kimmel, and G.Sapiro, "Geodesic active contours," *Intern. J. Comput. Vis.*, vol. 22, no. 1, pp. 61–79, 1997.

[12] D.Cremers, M.Rousson, and R.Deriche, "A review of statistical approaches to level set segmentation: Integrating color, texture, motion, shape," *Intern. J. Comput. Vis.*, vol. 72, no. 2, pp. 195–215, 2007.

[13] J.Weickert, B.Romeny, and M. Viergever, "Efficient and reliable schemes for nonlinear diffusion filtering," *IEEE Trans. Image Process.*, vol. 7, no. 3, pp. 398–410, Mar. 1998.

[14] M. Jeon, M. Alexander, W. Pedrycz, and N. Pizzi, "Unsupervised hierarchical image segmentation with level set and additive operator splitting," *Patt. Rec. Letters*, vol. 26, no. 10, pp. 1461–1469, Jul. 2005.

[15] M.Z.Brown, D.Burschka, and G.D.Hager, "Advances in computational stereo," *IEEE Trans. Pattern Anal. Machine Intell.*, vol. 25, no. 8, pp. 993–1008, Aug. 2003.